ADVANCED INTELLIGENT SYSTEMS
Open Access
www.advintellsyst.com

Color and Morphology Camouflaging using Biomimetic Scales

*Soroush Kamrava, Milad Tatari, Xinyu Feng, Ranajay Ghosh, and Ashkan Vaziri**

Due to obvious evolutionary advantages to both predator and prey, a rich gamut of camouflaging strategies exists in nature. Engineered camouflaging generally involves adapting bioinspired strategies to produce superior concealment and disguise in synthetic systems. Of special interest is dynamic, active camouflaging, which can rapidly conceal structures depending upon the background landscape. Herein, exciting advances are made by mimicking Cephalopod strategies. An alternative geometrically structured biomimetic scale-based strategy, which is purely mechanical and simple but at the same time rapid, tailorable and tunable, and inherently multifunctional, is presented. Surfaces covered by biomimetic scales that are themselves covered by lenticular images are investigated. A concurrent programming strategy to tune surface morphology and color by controlling the angle of individual scales is introduced. As an example, a pneumatic design to control individual-scale orientations using airflow, which enables both morphology and color camouflaging in less than a second, is demonstrated.

Camouflaging, which results in concealment and deception from external observation in nature, adds critical evolutionary advantage to both predators and preys. This mutual competition has resulted in a rich diversity of camouflaging strategies across various species.[1,2] In general, camouflaging commonly results in concealment when an animal's external appearance matches the background landscape or alters its appearance and shape, making it harder to identify (Crypsis). Another related strategy rests on changing the appearance to mimic another animal or a background object, such as leaf or twigs (Mimesis and Masquerade).[3] In addition to these strategies, animals can also make motion detection harder using special skin patterns (Motion dazzle) or move in a fashion that decrease chances of detection (Motion camouflage). Camouflaging can become especially effective if the animal can change its color to match the background landscape. This is seen in the case of several cephalopods, such as squid, cuttlefish, octopus (in general covering more than 700 species),[2,4] and chameleons.[5,6] This strategy allows the animals to traverse multiple diverse landscapes without becoming conspicuous. This active camouflaging strategy can be characterized by the time required to achieve concealment from a fully conspicuous state. In this, cephalopods exhibit the fastest camouflaging in nature using direct neural control.[7] Chameleons, on the other hand, change their skin color using a neurohormonal mechanism, which typically takes many seconds to few minutes.[6] Slower camouflaging is observed in golden tortoise beetles (2–3 min),[8] crab spiders (days to weeks),[9] and Corydalis Hemidicentra plant, which passively matches its color with that of the environment it grows in.[10]

Due to the striking visual outcome of camouflaging, its utility was understood by both hunters and militaries since the ancient times. Up until in the recent past, most of the visual military camouflaging techniques relied on passive strategies, such as coloring and external decorations, which were tailored for specific war theaters. However, modern, agile warfare puts premium on rapid and reliable camouflaging across a wide range of backgrounds, which would require actively controlled strategies. In past, Pikul et al.[11] presented a pneumatically actuated mechanism that could reversibly change its shape from a flat 2D surface to different 3D morphologies. They used pneumatic actuation to inflate a soft stretchable surface embedded with laser patterned inextensible layer to create a programmable surface morphology. Surface color tuning can also be achieved using thermochromic and eletrochromic materials,[12] strain induced technology,[13] colored pigment injection,[14] and electronic ink technology.[15] Electro-mechano-chemically responsive (EMCR) elastomer also enables creating large deformation patterns, color tuning, and emitting florescent signals on demand.[16] These currently available tunable synthetic camouflaging techniques can be broadly classified based on their use of either surface morphology and/or surface color and are shown in **Figure 1**A. The camouflaging time for these engineered camouflaging strategies for changing color can be put in perspective with their natural counterparts and are shown in Figure 1B.

These impressive advances in dynamic concealment strategies are possible mainly due to advances in synthetic-engineered

S. Kamrava, M. Tatari, X. Feng, Prof. A. Vaziri
Mechanical and Industrial Engineering Department
Northeastern University
360 Huntington Ave, Boston, MA 02115, USA
E-mail: vaziri@coe.neu.edu

Prof. R. Ghosh
Department of Mechanical and Aerospace Engineering
University of Central Florida
12760 Pegasus Drive, Orlando, FL 32816, USA

The ORCID identification number(s) for the author(s) of this article can be found under https://doi.org/10.1002/aisy.201900021.

DOI: 10.1002/aisy.201900021

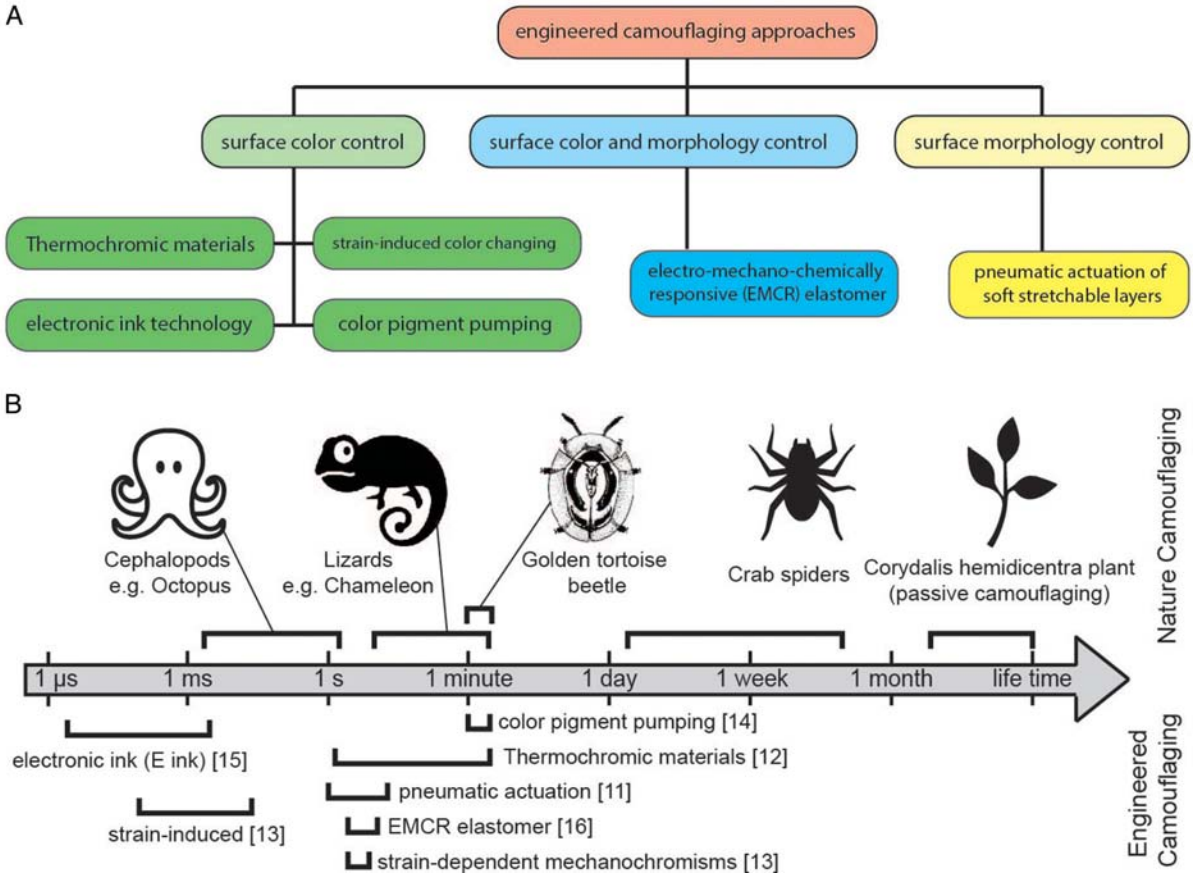

Figure 1. A) Broad classification of current engineered camouflaging strategies based on the control of color, surface morphology, or both. B) A comparative characteristic time diagram contrasting camouflaging strategies commonly found in nature with currently proposed engineered camouflaging. The characteristic time is the average time taken for the surface to change from its reference conspicuous state to fully concealed state. The natural mechanisms with schematic of a representative organism are on the top of the time arrow whereas the time scales of engineered camouflaging are depicted in the bottom.

camouflaging materials, which combine pigment or soft surface morphology. In contrast to these purely material-based strategies, in this paper, we explore a topology-based strategy by utilizing biomimetic scales for tunable/tailorable dynamic camouflaging. Biomimetic scales, which are inspired by fish scales, have already been used to generate geometrically tailorable mechanical properties.[17] Therefore, this biomimetic scale-based strategy is inherently a multifunctional design.

In nature, scales are commonly used by some fishes for visual evasion by reflecting incoming light (typically nondirectional due to scattering from water borne particles[18]) and structural coloration of Lepidoptera wings as a result of coherent light scattering by the photonic crystal nature of the scales.[19] However, these are passive strategies and not suitable for changing colors on demands. In this article, using lenticular flip images and scale actuation, we develop a robust camouflaging method for tuning both surface morphology and color by changing scale inclination. Despite the relative simplicity and multifunctional benefits of this framework, the programmability can be achieved within seconds, on par with many existing techniques.

We devised a pneumatic actuation system to control the angle of individual scales that enables achieving fast surface camouflaging (in the order of seconds). The biomimetic scale system is an array of rectangular plates $(L \times t)$ capable of freely rotating around a fixed axis on a substrate. **Figure 2**A shows the geometry of a sample 3D printed set of eight biomimetic scales situated on a substrate. θ_i is the angle measured between the ith scale and the horizontal line on the substrate. The distance between ith and $i+1$th scale is denoted as d_i. Using a suitable actuation method, individual scales can be brought into certain configurations by changing θ_i, which can result in various surface morphologies along the surface of the biomimetic scale system. The bottom row of Figure 2A shows two examples of different surface morphologies, where the biomimetic scales with $L = 20$ mm and $d = 10$ mm are positioned in such a way that the tip of scales approximates a bumped shape and an inclined surface, respectively. To approximate a certain morphology (target function) using biomimetic scales (fixed L, and d_i), an inverse problem must be solved to obtain the desired value of θ_i for each scale. A computer code was used to find the desired values of θ in a biomimetic scale set with fixed d_i and L. Algorithmically, the target function (defining the required morphology) was intersected with n circles with a radius of L (length of scales) and centers on the axis of rotation of the scales. This is shown in

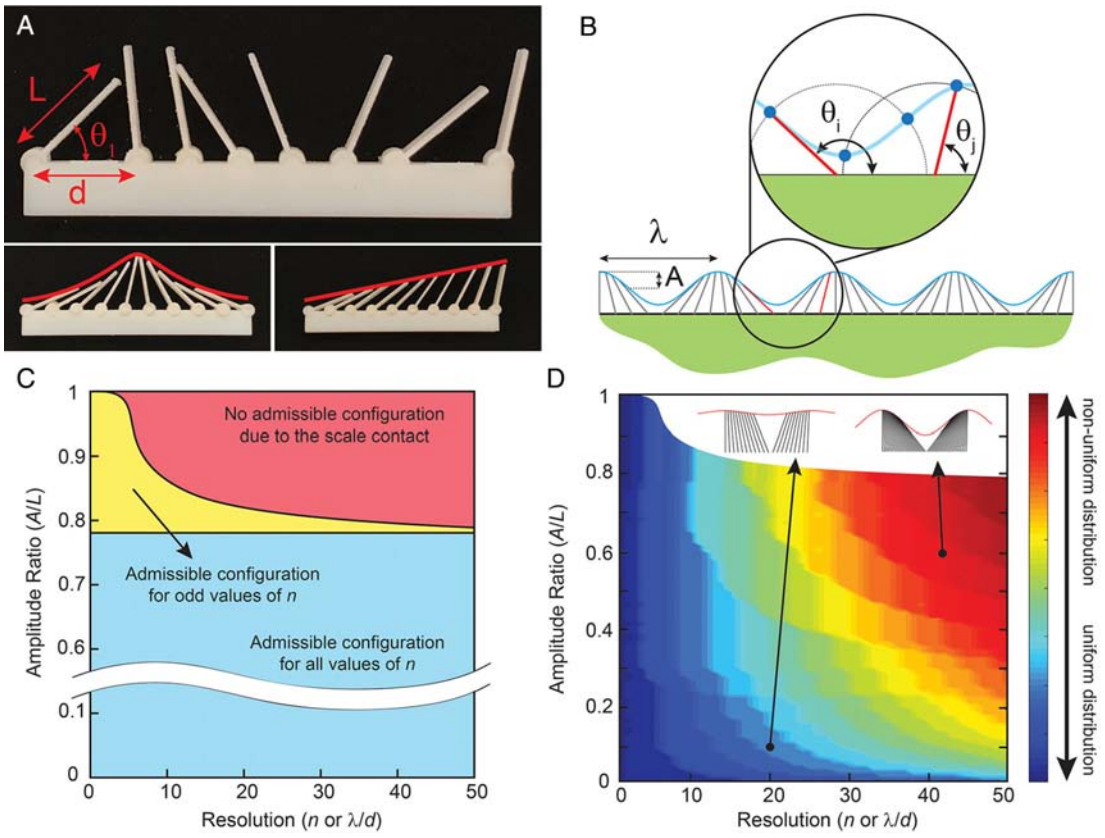

Figure 2. A) A 3D printed biomimetic scale array with eight scales with tunable scale angle θ_i, which is the angle between ith scale and the substrates. The length of the ith scale and the distance between ith and $i+1$th scales are indicated as L_i and d_i, respectively. Individual scales can be brought into certain configurations by changing θ_i, which can result in various surface morphologies. In the two given examples below, the biomimetic scales with $L = 20$ mm and $d = 10$ mm are positioned in such a way that tip of scales can approximate a symmetric curvilinear shape and an inclined surface. B) An array of identical biomimetic scales approximating sinusoidal function $y = A\cos(\frac{2\pi x}{\lambda})$ depicting wavelength λ and amplitude A. The individual-scale configuration was determined using a computer code and among all possible configurations, one with the minimum number of interesting scales was chosen. C) Phase map illustrating the availability of valid solution for an array of $n(0 \leq n \leq 50)$ scales approximating the function of $y = A\cos(\frac{2\pi x}{\lambda})$ from $x = 0$ to 2π mapped by resolution (λ/d) and nondimensional amplitude ratio (A/L). The map shows three regions encompassing, admissible solutions for any number of scales (blue), admissible solutions for odd number of scales (yellow), and no admissible solutions (red). D) Distribution uniformity plot using Pearson's chi-squared test mapped via resolution (λ/d) and amplitude ratio (A/L).

Figure 2B for a sinusoidal target function $y = A\cos(\frac{2\pi x}{\lambda})$, where A is the amplitude and λ is the wavelength. We acknowledge that this procedure may result in multiple θ values of each scale. However, uniqueness is imposed by choosing a value of θ close to 90° (normal line to the substrate), which gives more angular freedom than the neighboring scales and results in a more uniform scale distribution.

In addition, unphysical mathematical solutions where scales penetrate into each other are deemed inadmissible. Two natural nondimensional parameters define the envelopes of admissible solutions. The amplitude of the sinusoid gives us the first nondimensional parameter, $A/L < 1$ (amplitude ratio). The other parameter arises from comparing the wavelength of the sinusoid with the scale spacing. It can be expected that if scales are spaced too close together, compared with the wavelength, sufficient angular freedom may not be available before they contact each other. This gives rise to the parameter $n = \lambda/d$ (resolution). Using these two parameters, an admissibility phase map may be constructed, as shown in Figure 2C. The phase map is produced numerically using the earlier described computer code. Three different colors of blue, yellow, and red correspond to, respectively, the areas of admissible configuration for all values of n, admissible configuration only for odd values of n, and no admissible configuration due to the scale contact. As shown in the phase map, for $0 < n \leq 50$ and $A/L < 0.78$, it is always possible to achieve an admissible configuration, which perfectly fits the target function of $y = A\cos(\frac{2\pi x}{\lambda})$. On the other hand, as n increases, the admissible region for odd n values diminishes for $A/L > 0.78$.

Interestingly, although a large number of admissible scale designs are possible for a given morphology, their uniformities differ. Uniformity in distributing scale tips over the target function affects the quality of morphology and thus camouflaging itself. Uniformity can be quantified using the Pearson's chi-squared test, which compares the distribution of counts for two or more groups.[20] The level of uniformity in the scale distribution of a certain scale system can be calculated by applying Pearson's test between a particular scale configuration and a

uniformly distributed set. First, the target function is divided to N equal cells over the x axis, and then, the value of Pearson's chi-squared test for such a case can be obtained from Equation (1)

$$\chi^2 = \sum_{i=1}^{N} \frac{(O_i - \frac{n}{N})^2}{\frac{n}{N}} \tag{1}$$

where χ^2, n, O_i, and N are the value of Pearson's test, number of scales, number of scale tips in the ith cell, and number of cells, respectively. The χ^2 is zero for an ideally uniform distributed scale set and χ^2 increases as the concentration of scale tips increases or decreases locally. Figure 2D shows a contour plot, which describes the uniformity of scale distribution over the target function of $y = A\cos(\frac{2\pi x}{\lambda})$ using the Pearson's chi-squared test, where number of cells (N) is equal to number of scales (n), mapped by A/L and $n(\text{or } \lambda/d)$. Two insets of Figure 2D show two different levels of uniformity in the distribution of biomimetic scales over the target function. The phase map shows that uniformity improves for longer and more sparsely placed scales. Alternatively, for a given configuration of scales, morphologies with lower amplitude and shorter wavelengths produce greater uniformity. In contrast, shorter and closely spaced scales are expected to produce a more textured appearance. However, there is a limit of packing scales too closely together as that would affect their motion and restrict tunability. Assuming a constant target function, having a more refined pattern with uniformly distributed scales requires smaller λ/d and A/L, which can be achieved through scaling down the entire scale set (i.e., decreasing the values of L and d).

These investigations clearly demonstrate the tailorability of shape and the morphology of surfaces using a scale-based design. By incorporating an actuating mechanism on the scales' base, which can lead to rotation, this tailorable morphology can be used to produce tunable textured colors on the surfaces using lenticular flip images. The lenticular flip image allows the viewer to see different images depending on the viewing angle.[21] The lenticular image is made of a layer of graphic consisting two different images (solid colors here) interlaced together and a layer of lenticular lens on top,[22] see **Figure 3**A. The lenticular lens, a plastic sheet covered by parallel lenticulas (semi-cylindrical lenses), acts as a magnifying glass and displays only a portion of the interlaced graphic located underneath the lens depending on the viewing angle.[21,23] In the case shown in Figure 3A, each lenticula has precisely located on the top of two red and yellow strips (width of each color strip is half the width of lenticula), and the maximum viewing angle of the lenticular lens is α (i.e., a calculated angle in which the lenticular lens delivers a correct

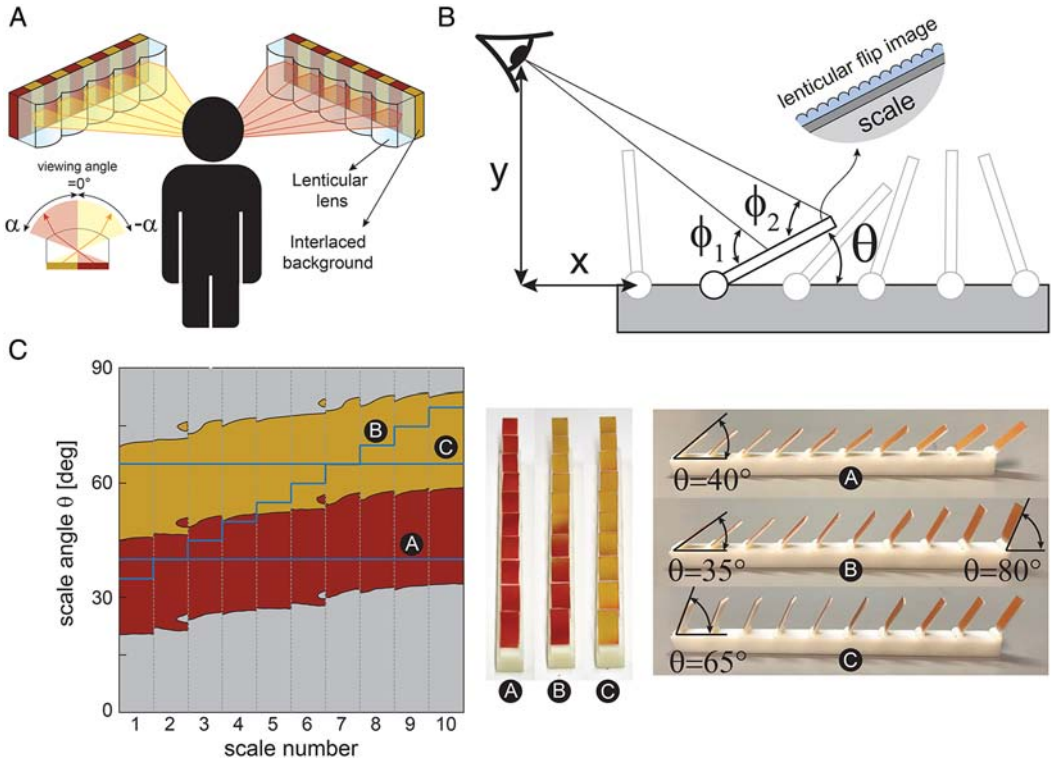

Figure 3. A) Lenticular flip images are made of an interlaced background image and a sheet of lenticular lens, which delivers different images while looking at them at different viewing angles. Here, a lenticular image was fabricated with two phases of yellow and red solid colors. B) Principles of color tuning where covering the surface of each biomimetic scale by the red/yellow lenticular images enables tuning the color of scales based on the position of the observer. C) Color appearance of a biomimetic scale array containing ten scales from the sight of an observer located at $x = y = 30$ cm. The horizontal axis shows the scale number starting from the closest scale to the observer and the vertical axis is the angle θ for each scale. The color programmability of the biomimetic scale is demonstrated through three examples of *A*, *B*, and *C*, where sample A is entirely red, sample B is partially red and yellow, and sample C is entirely yellow (see the corresponding lines to each example on the color map on the left).

picture). If the observer looks at the lenticular flip image at a viewing angle between $-\alpha^\circ$ and α° (measured from the normal line to the image surface), either red or yellow color delivers to the eyes and color changes (from red to yellow or yellow to red) when the observer passes the normal line. This maximum viewing angle α is a property of the lenticular lens system and fixed for a given design. It is noted that the lenticular images can be used for delivering multiple colors by reducing the width of each color strip on the graphical background located underneath of the lenticular lens. In this article, we used only two colors of yellow and red to create a simple demonstration of the concept. Figure 3B shows the side view of an observer looking at a biomimetic scale system with scales covered by lenticular flip images, while the horizontal and vertical distances between the observer and the first scale are denoted as x and y, respectively. In this configuration, clearly the viewing angle is not a constant for all the scales. For example, the viewing angle for the second scale has a value between $90^\circ - \phi_1$ and $90^\circ - \phi_2$ (measured from the normal line). As shown in Figure 3A, we can develop a mapping between the viewing angle and the appearing color, in which the observers with viewing angles between $-\alpha^\circ$ and 0° receive the yellow color and the observers with viewing angles between 0° and α receive the red color.

A MATLAB-based computer code is used to calculate the viewing angle for an array of n biomimetic scales based on the geometrical parameters of x, y, d, L, and n, and variable θ and then find the appearing color of each scale based on the explained mapping principle. The results presented in Figure 3C are extracted from the code with $x = y = 30$ cm, $L = 2$ cm, $d = 2$ cm, and $n = 10$. The horizontal axis indicates the scale number (counting from left to right), and the vertical axis is the scale orientation (θ). According to the plot, the appearing color of scales for a certain morphology can be found using the scale number and angle θ. To validate the numerical results, an array of ten biomimetic scales covered by lenticular flip images with $\alpha = 24.5^\circ$ and lenticulas per unit inch LPI = 60 (width of each lenticula is 1/60 inches) were 3D printed. Three different scale systems are used, denoted as A, B, and C shown on the right side of Figure 3C. In configuration A and C, all θ values are constant and equal to 40° and 65°, respectively, and θ value in the configuration B increases linearly from 35° to 80° along the length of the substrate. The color texture is shown in Figure 3C (extreme left) where the vertical axis denotes the scale angle and horizontal axis denotes the scale number starting from the viewing end. The color patches for each scale show the predicted extent of the range of colors visible to the observer for that scale depending on the angle of the scale. Using the scale angles for a given scale, all three samples A, B, and C have been superimposed on this plot. As the scale angles are constant for samples A and C, they are straight horizontal lines on this plot, fully inside the red and yellow region, respectively. At the same time, the functionally graded scales of sample B with varying scale angles start from the red region and then moves into the yellow region as with more distant scales. The transition begins to occur around the fourth scale and completes by the sixth. The observer's view of three samples shows an excellent agreement between the experimental result and the analytical results presented in the plot. Therefore, using this model, it is possible to design a programmable tunable system, which can deliver precise surface texture through a scale angle controller. A fully functional camouflaging system requires a feedback system, such as motion camera, to sense the location of observer and deliver the desired color accurately. However, developing such a feedback-controlled system is out of the scope of this article, and intelligence will be achieved once camera is installed on the structure. The camouflaging time for such a mechanism would depend on the actuation method employed. In this work, a pneumatic tunable system is introduced, which is both simple and reasonably fast (camouflage time $\approx$s). The proposed camouflaging system has been designed and analyzed in a 2D space, which narrows down the range of possible applications of this system. However, the similar principles can be used in conjunction with directional lenticular lenses, which can deliver the desired images in a 3D space,[24] to improve this limitation in the proposed camouflaging system.

In this section, a tunable surface coloration concept is demonstrated. From the earlier discussion, it is clear that both morphology and color camouflaging of the biomimetic scale set can be controlled by the rotation of scales. Thus, tunability can be achieved using an actuation method to control the angle of individual scales. Here, an air-controlled scale design in which the angle θ of each scale can be tuned through changing an incoming airflow is experimentally demonstrated. **Figure 4**A shows the side view of the scale design with two air inlets and one scale able to rotate freely. Air inlets are connected to air cavities, which are separated from each other using the moving scale. Increasing the air pressure in either sides of the scale (pressurizing take place through connecting air inlets to an airflow) moves the scale to the opposite direction, as connecting the flow to inlet 1 and inlet 2 moves the scale to the right and left, respectively. Also, two small holes are located on the top surface of the air cavities to regulate air pressure through letting some air out. Figure 4B shows five different scale configurations of a 3D printed air-controlled scale. These configurations can be achieved through manipulating the airflow entering the air inlets. In two extreme left and right cases, the pressure in one of the air cavities is higher than the other because of substantially different airflow rates entering two inlets. In this case, the scale goes to the extreme left or right positions due to the unequal applied forces on two sides of the scale. To position the scale in between the extreme configurations, the air pressure on the both cavities should be equal, which provides a zero effective applied force to the scale. In case of equal airflow entering the left and right cavities, the scale goes to the vertical configuration due to the symmetry (third image). If the incoming airflow to inlet 1 is slightly greater than inlet 2, the scales moves to the right until it reaches and blocks one of the pressure regulation holes. In this configuration, the extra airflow entering inlet 1 leaves the air cavity through the left pressure regulation hole and the scale rests at the balanced pressure on both sides (fourth image from left). Same principles apply when the airflow to inlet 2 is slightly greater than inlet 1 and moves the scale to the left until it reached the left pressure regulation hole (second image from left). Increasing the number of pressure regulation holes improves the accuracy of scale orientation control through adding additional equilibrium positions. Please see Movie 1, Supporting Information, for more details on the performance of the air-controlled scale. Figure 4C shows an array of ten

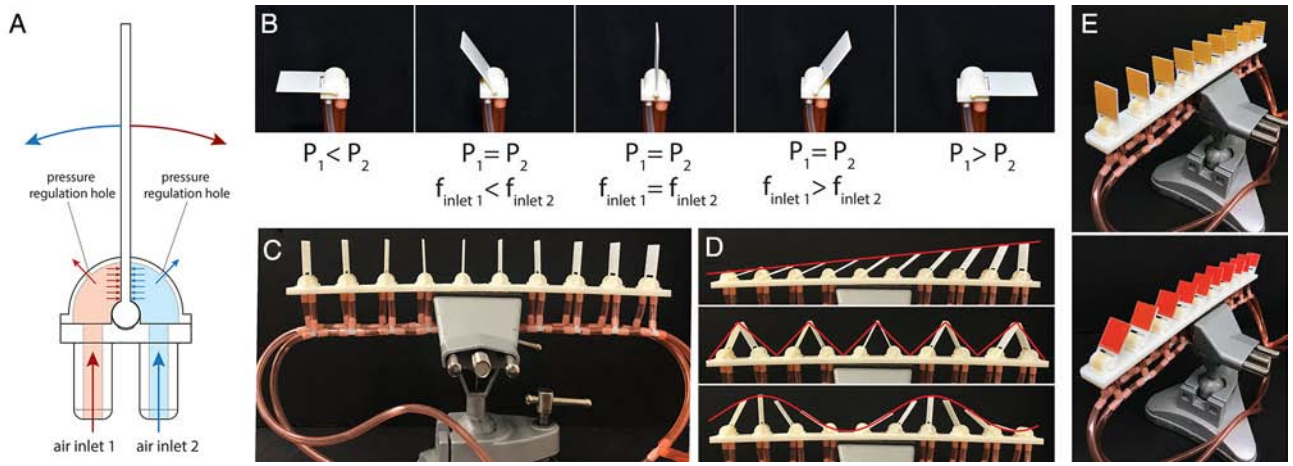

Figure 4. A) A schematic of the cross section of air-driven scale where pressurizing each inlet causes the rotation of scale in the opposite direction. The pressure regulation holes on the top of the circular part provide two additional equilibrium configuration for the tunable scale. B) Five possible configurations of 3D printed air-driven scale, which can be achieved through changing the incoming airflow to each inlet. C) A 3D printed array of 10 scales in which all scales are pneumatically coupled and controlled simultaneously. D) Inclined, zig–zag, and sinusoidal morphologies created by controlling individual scales rather than simultaneous control of all scales. E) Air-driven biomimetic scales exhibit different colors at two different configurations from the same viewing position (see Movie 2, Supporting Information, for more details).

air-controlled 3D printed scales placed on a substrate. All scales are pneumatically coupled, meaning that inlet 1 of all scales is connected to each other using tubes and same for inlet 2. Movie 2, Supporting Information, shows the actuation of air-controlled biomimetic scale array using a single air source. More complicated patterns can be created by controlling individual scales rather than using the pneumatically coupled scales. Figure 4D demonstrates three different morphologies of inclined, zig–zag, and sinusoidal surfaces, which can be achieved through the actuation of individual scales in an array. In addition to the morphology tuning, the visible color of biomimetic scale array can be tuned using the air-controlled scales. Covering the surface of scales in the same array, as shown in Figure 4C, using the lenticular flip images provides control on the color of biomimetic scale array. Figure 4E shows the biomimetic scale array configured in different shapes, which causes different colors in the observer's eyes. Please see Movie 2, Supporing Information, for more details on the color tuning of biomimetic scales. Although only uniform angular change has been demonstrated, the concept can be extended readily to obtain individual-scale angle control, which would result in a rich color texture and more intricate control.

In conclusion, a novel tailorable/tunable biomimetic scale-based system capable of both surface morphology and color camouflaging has been investigated. Although the best result can be achieved through programming either color or morphology by controlling the orientation of individual scales, it is noted that the solution for color or morphology camouflaging is not unique and we may use the orientations, which satisfy both the morphology and color requirements. The color pattern was based on using lenticular flip images to tune the observed color of the biomimetic scale set through changing the orientation of individual scales. A tunable design was proposed using air-controlled 3D printed scale in which the orientation of scale was precisely controlled using airflow. This air-controlled programmable design enabled a fairly reliable, fast, and simple morphology production and color camouflaging system. In contrast to other techniques of active camouflaging, a scale-based design provides a framework for designing potentially multifunctional structures, as shown in the previous literature. The fundamental principles of this mechanical system are more general. For instance, origami-based structures[25] such as the origami string with shape programmability[26] can also be used as a low-cost alternative method for controlling the complex geometries of engineered camouflage systems because of the limited number of required actuators or using a shape-memory composites in hinges to control the scale orientation by changing the temperature.[27] At the end, the proposed camouflaging system can be used in conjunction with soft substrate and flexible air tubes connecting scales to each other, which make the proposed system a great fit for soft robotic applications.[28]

Experimental Section

Scales and substrate were designed in SolidWorks (Dassault Systemes), fabricated separately using PolyJet 3D printing technique (Objet Eden260V 3D printer, Stratasys Inc., Eden Prairie, MN), and assembled by hand in a way that scales can rotate freely around their rotation axis. Each air-controlled scale was composed of three different sub-parts of scale, upper cap of cavity, and lower cap of cavity. These three components were 3D printed using the same technology and assembled to form a functional tunable scale system. The air pressure inside both air cavities was measured using a pressure sensor (HSCDRRN005PD2A5, Honeywell Inc., Morris Plains, New Jersey, United States) connected to two air cavities; the sensors measured the pressure difference on both sides of the scale. An ARDUINO UNO REV3 was used to program the sensor and display the results. The lenticular image was made up of a layer of graphic consisting two interlaced colors, created by Adobe Illustrator and printed using a commercial color jet printer, and a layer of 60 LPI flip lenticular plastic lens (Lenstar Plus, United State) on top.[22] The graphic image was attached to the lens using double-sided tape and then glued to the 3D printed scale.

Supporting Information

Supporting Information is available from the Wiley Online Library or from the author.

Acknowledgements

This work is supported by the United States National Science Foundation, Division of Civil, Mechanical, and Manufacturing Innovation, Grant No.1634560.

Conflict of Interest

The authors declare no conflict of interest.

Keywords

biomimetic scale, camouflage, lenticular image, soft robotics, tunable color, tunable morphology

Received: May 9, 2019
Revised: June 17, 2019
Published online: July 8, 2019

[1] a) G. H. Thayer, *Concealing-coloration in the animal kingdom: an exposition of the laws of disguise through color and pattern: being a summary of Abbott H. Thayer's discoveries*, Macmillan Company, London, **1918**; b) H. B. Cott, *Adaptive coloration in animals*, Methuen, London, **1940**; c) E. B. Poulton, *The colours of animals: their meaning and use, especially considered in the case of insects*, D. Appleton, New York, **1890**; d) Aristotle, *Aristotle's History of Animals: In Ten Books*, BiblioBazaar, LLC, Charleston, **2008**; e) A. H. Thayer, *Auk* **1896**, *13*, 124; f) J. N. Lythgoe, *The ecology of vision*, Oxford University Press, Oxford, **1979**.

[2] R. T. Hanlon, J. B. Messenger, *Phil. Tran. R. Soc. Lond. B Biol. Sci.* **1988**, *320*, 437.

[3] M. Stevens, S. Merilaita, *Animal camouflage: mechanisms and function*, Cambridge University Press, Cambridge, **2011**.

[4] a) R. T. Hanlon, J. B. Messenger, *Cephalopod behaviour*, Cambridge University Press, Cambridge, **2018**; b) R. T. Hanlon, M.-J. Naud, J. W. Forsythe, K. Hall, A. C. Watson, J. McKechnie, *Am. Nat.* **2007**, *169*, 543; c) R. Hanlon, C.-C. Chiao, L. Mäthger, A. Barbosa, K. Buresch, C. Chubb, *Philos. Trans. R. Soc. B Biol. Sci.* **2008**, *364*, 429; d) R. Hanlon, *Curr. Biol.*, **2007**, *17*, R400.

[5] D. Stuart-Fox, A. Moussalli, M. J. Whiting, *Biol. Lett.* **2008**, *4*, 326.

[6] J. T. Bagnara, M. E. Hadley, *Chromatophores and color change: the comparative physiology of animal pigmentation*, Prentice-Hall, Englewood Cliffs, N.J, **1973**.

[7] E. Kreit, L. M. Mäthger, R. T. Hanlon, P. B. Dennis, R. R. Naik, E. Forsythe, J. Heikenfeld, *J. R. Soc., Interface*, **2013**, *10*, 20120601.

[8] E. M. Barrows, *Coleopt. Bull. 33*, **1979**, 9.

[9] L. Chittka, *Entomol. Gen.* **2001**, *25*, 181.

[10] a) Y. Niu, Z. Chen, M. Stevens, H. Sun, *Proc. R. Soc. B*, **2017**, *284*, 20171654; b) Y. Niu, G. Chen, D. L. Peng, B. Song, Y. Yang, Z. M. Li, H. Sun, *N. Phytol.* **2014**, *203*, 953.

[11] J. Pikul, S. Li, H. Bai, R. Hanlon, I. Cohen, R. Shepherd, *Science* **2017**, *358*, 210.

[12] a) K. Karpagam, K. Saranya, J. Gopinathan, A. Bhattacharyya, *J. Text. Inst.* **2017**, *108*, 1122; b) C. Yu, Y. Li, X. Zhang, X. Huang, V. Malyarchuk, S. Wang, Y. Shi, L. Gao, Y. Su, Y. Zhang, *Proc. Natl. Acad. Sci.* **2014**, *111*, 12998; c) R. Zheng, Y. Wang, C. Jia, Z. Wan, J. Luo, H. A. Malik, X. Weng, J. Xie, L. Deng, *ACS Appl. Mater. Interfaces* **2018**, *10*, 35533; d) G. A. Sotzing, J. L. Reddinger, A. R. Katritzky, J. Soloducho, R. Musgrave, J. R. Reynolds, P. J. Steel, *Chem. Mater.* **1997**, *9*, 1578; e) R. C. Shallcross, P. O. Körner, E. Maibach, A. Köhnen, K. Meerholz, *Adv. Mater.* **2013**, *25*, 4807.

[13] a) S. Zeng, D. Zhang, W. Huang, Z. Wang, S. G. Freire, X. Yu, A. T. Smith, E. Y. Huang, H. Nguon, L. Sun, *Nat. Commun.* **2016**, *7*, 11802; b) T. Yang, Y. Zhong, D. Tao, X. Li, X. Zang, S. Lin, X. Jiang, Z. Li, H. Zhu, *2D Mat.*, **2017**, *4*, 035020.

[14] S. A. Morin, R. F. Shepherd, S. W. Kwok, A. A. Stokes, A. Nemiroski, G. M. Whitesides, *Science* **2012**, *337*, 828.

[15] B. Comiskey, J. D. Albert, H. Yoshizawa, J. Jacobson, *Nature* **1998**, *394*, 253.

[16] Q. Wang, G. R. Gossweiler, S. L. Craig, X. Zhao, *Nat. Commun.* **2014**, *5*, 4899.

[17] a) R. Ghosh, H. Ebrahimi, A. Vaziri, *Appl. Phys. Lett.* **2014**, *105*, 233701; b) R. Ghosh, H. Ebrahimi, A. Vaziri, *J. Mech. Behav. Biomed. Mater.* **2017**, *72*, 1; c) R. Ghosh, H. Ebrahimi, A. Vaziri, *EPL (Europhys. Lett.)* **2016**, *113*, 34003; d) H. Ali, H. Ebrahimi, R. Ghosh, *Int. J. Solids Struct.* **2019**.

[18] D. Gur, B. Leshem, D. Oron, S. Weiner, L. Addadi, *J. Am. Chem. Soc.* **2014**, *136*, 17236.

[19] a) S. Kinoshita, S. Yoshioka, Y. Fujii, N. Okamoto, *Forma-Tokyo*, **2002**, *17*, 103; b) C. W. Mason, *J. Phys. Chem.* **1927**, *31*, 321.

[20] D. Bock, P. Velleman, R. De Veaux, *Stats: Modeling the world: AP Edition*, Addison Wesley, Boston, MA, **2010**.

[21] L. A. Bowen, C. L. Grames, S. P. Magleby, L. L. Howell, R. J. Lang, *J. Mech. Design* **2013**, *135*, 111008.

[22] D. Kessler, L. W. Tutt, Google Patents, **2001**.

[23] E. R. Sandor, W. T. Cunnally, S. B. Meyers, Google Patents, **1996**.

[24] J. A. Magee, Google Patents, **2004**.

[25] a) S. Kamrava, D. Mousanezhad, H. Ebrahimi, R. Ghosh, A. Vaziri, Scientific Reports **2017**, *7*; b) D. Mousanezhad, S. Kamrava, A. Vaziri, Scientific Reports **2017**, *7*, 14792; c) S. Kamrava, R. Ghosh, Z. Wang, A. Vaziri, *Adv. Eng. Mater.* **2019**, *21*, 1800895.

[26] a) S. Kamrava, D. Mousanezhad, S. M. Felton, A. Vaziri, *Adv. Mater. Technol.* **2018**; b) S. Kamrava, R. Ghosh, Y. Yang, A. Vaziri, *EPL (Europhys. Lett.)* **2018**, *124*, 58001.

[27] M. T. Tolley, S. M. Felton, S. Miyashita, D. Aukes, D. Rus, R. J. Wood, *Smart Mater. Struct.* **2014**, *23*, 094006.

[28] a) D. Rus, M. T. Tolley, *Nature* **2015**, *521*, 467; b) A. D. Marchese, C. D. Onal, D. Rus, Soft Robotics **2014**, *1*, 75; c) M. Tatari, A. Mohammadi Nasab, K. T. Turner, W. Shan, *Adv. Mater. Interfaces* **2018**, *5*, 1800321; d) A. M. Nasab, A. Sabzehzar, M. Tatari, C. Majidi, W. Shan, *Soft Robot.* **2017**, *4*, 411.